Dissociable Cerebellar-Prefrontal Networks Underlying Executive Function:

Evidence from the Human Connectome Project

Running title: CB-PFC networks underlying executive function

Joseph M. Orr*[a,b], Trevor B. Jackson[a],Michael J. Imburgio[a], & Jessica A. Bernard*[a,b]

[a]Department of Psychological and Brain Sciences,

[b]Texas A&M Institute for Neuroscience,

Texas A&M University

College Station, TX 77843

*Corresponding Author:

Joseph M. Orr or Jessica A. Bernard

515 Coke Street

4235 TAMU

College Station, TX 77843-4235

Email: joseph.orr@tamu.edu or

jessica.bernard@tamu.edu

Acknowledgements

Abstract

To date, investigations of executive function (EF) have focused on the prefrontal cortex (PFC), and prominent theories of EF are framed with respect to this brain region. Multiple theories describe a hierarchical functional organization for the lateral PFC. However, recent evidence has indicated that the cerebellum (CB) also plays a role in EF. Posterior CB regions (Crus I & II) show structural and functional connections with the PFC, and CB networks are associated with individual differences in EF in healthy adults. However, it is unclear whether the cerebellum shows a similar functional gradient as does the PFC. Here, we investigated high-resolution resting-state data from 225 participants in the Human Connectome Project. We compared resting-state connectivity from posterior cerebellar ROIs, and examined functional data from several tasks that activate the lateral PFC. Demonstrating preliminary evidence for parallel PFC and CB gradients, Crus I was functionally connected with rostrolateral PFC, Crus II with middle and ventral PFC, and Lobule VI with posterior PFC. Contrary to previous work, the activation of the task thought to activate rostrolateral PFC resembled the connectivity maps of Crus II, not Crus I; similarly, the activation of the task thought to activate middle PFC resembled the connectivity maps of Crus I, not Crus II. Nevertheless, there was evidence for dissociable CB-PFC networks. Further work is necessary to understand the functional role of these networks.

Keywords

executive function, cerebellum, prefrontal, functional connectivity, fmri

Introduction

As we navigate our day to day lives, intact executive function (EF) plays a critical role in educational, work, and home settings. EF allows for us to fluidly update our goals and the appropriate behavioral responses online. Indeed, across psychiatric disorders, EF deficits are a prominent feature and contribute to declines in quality of life. EF deficits are thought to be at the core of diseases such as schizophrenia [e.g., Kerns et al., 2008], depression [Snyder, 2013], and substance abuse [Volkow et al., 2011]; this underscores the importance of a clear and complete understanding of this critical cognitive domain. We know that the prefrontal cortex (PFC) plays a crucial role in EF [Miller and Cohen, 2001], and the prominent theories of the neural underpinnings of EF are focused on the PFC.

Nevertheless, the PFC does not act alone, and several cortical (e.g., parietal) and subcortical (e.g., thalamus and striatum) regions have strong connections with the PFC. While PFC-thalamic and PFC-striatal loops are well characterized and integrated into theories of EF [Alexander et al., 1986; Masterman and Cummings, 1997], the connections between the PFC and cerebellum [Bernard et al., 2012; Bernard et al., 2014; Bernard et al., 2016; Kelly and Strick, 2003; Salmi et al., 2010] and their role in EF, are less understood. While the suggestion that the cerebellum may play a role in non-motor behavior is not a new idea [Leiner et al., 1986; Leiner et al., 1993; Schmahmann and Sherman, 1998], more recently there has been an increase in evidence to support this idea more directly. Investigations in non-human primates have revealed distinct closed-loop circuits connecting anatomically segregated regions of the cerebellum and motor and prefrontal cortices, respectively [Dum and Strick, 2003; Kelly and Strick, 2003], and these segregated circuits have also been replicated in the human

brain with both structural [Bernard et al., 2016; Salmi et al., 2010] and functional [Bernard et al., 2012; Bernard et al., 2014; Krienen and Buckner, 2009; O'Reilly, 2010] measures of brain connectivity. While some investigations have directly compared connectivity between lobules at rest, these investigations have focused on sensorimotor function [Kipping et al., 2013] or associations with known cortical networks [Sang et al., 2012]. Importantly however, Sang and colleagues did suggest heterogeneity in the connectivity patterns of the posterior aspects of the cerebellum. Further, meta-analytic connectivity modelling has suggested co-activation between Crus I and II of the cerebellum and prefrontal cortical regions during task performance [Balsters et al., 2014] providing further support for the purported importance of these regions in EF. Direct comparisons of the connectivity patterns of Crus I and II are thus warranted for our understanding of the cerebellum in EF, and to better elucidate whether a similar functional processing gradient exists in both the cerebellum and PFC.

Paralleling the closed-loop circuitry of the cerebellum, lateral posterior regions of the cerebellum have been implicated in cognitive processing. Early work in patients with cerebellar lesions demonstrated both cognitive and affective deficits in patients with posterior cerebellar lesions [Schmahmann and Sherman, 1998]. More recently, work using functional imaging has suggested a corresponding functional topography in the cerebellum [e.g., E et al., 2012; Stoodley et al., 2012; Stoodley and Schmahmann, 2009]. Lateral posterior lobules of the cerebellum (Crus I, Crus II), show activation during the performance of cognitive tasks, including EF tasks. This parallels the regions of the structure showing both structural and functional connections with the PFC [Bernard et al., 2012; Bernard et al., 2016; Krienen and Buckner, 2009; O'Reilly et al., 2010; Salmi et al., 2010]. However, the specific contribution these posterior lobules make to

cognitive behavior remains unknown. It has been suggested that much like in the motor domain, Crus I and Crus II of the cerebellum process internal models of thought, that aid in, and allow for organized and efficient cognition [Ito, 2008; Ramnani, 2006]. More recently, Ramnani [2014] has suggested that connections between the PFC and cerebellum support the trade-off or transition during cognitive learning from top-down control to automatic processing according to internal models. With that said, it may be the case that these regions differentially contribute to distinct components of EF, subserved by their connectivity patterns with the prefrontal cortex.

There are a number of theories describing the functional organization of the PFC. Many of these theories suggest that the PFC is organized in a rostral-caudal gradient of abstraction [Badre, 2008; O'Reilly, 2010], and as such, different regions of the PFC contribute to different components of EF. The most anterior aspects of the PFC (rostral lateral prefrontal cortex; RLPFC) are thought to be involved in abstract higher order behaviors like the control of multiple goals, prospective memory, or using internal goals to guide task selection [Burgess et al., 2007; Koechlin and Hyafil, 2007; Orr and Banich, 2014]. Conversely, the more posterior regions of the PFC (i.e., premotor cortex and inferior frontal gyrus) are thought to be involved in more concrete behaviors related to action, including sensory or response selection [Banich, 2009]. While some accounts suggest this abstraction gradient is hierarchical (with the RLPFC being at the apex), more recent evidence suggests that the dorsolateral PFC (DLPFC) is the apical region of the PFC. Regardless of the nature of this organization, intact PFC function is thought to be necessary for maintaining healthy EF. However, the PFC is unlikely to be acting alone. A network-based approach to understanding EF is crucial, and in particular, an eye towards the cerebellum is warranted.

To investigate cerebellar-prefrontal networks, we utilized data from 225 neurotypical unrelated participants in the Human Connectome Project (HCP), due to its large size and exceptional data quality—ultra-high resolution (0.7 mm isotropic) structural images, high-resolution fMRI scans (3 mm isotropic)—from a variety of cognitive, emotion, and motor tasks, and multiple sessions of resting-state fMRI (rfMRI). Data in the HCP comes from a healthy young adult (21-35 years) community sample. We focused on rfMRI data for the current study in order to identify dissociable cerebellar-prefrontal networks. Cerebellar regions-of-interest were defined from the SUIT Probabilistic atlas [Diedrichsen et al., 2009]. We selected three lateral posterior cerebellar regions from the left and right hemispheres: Crus I, Crus II, and Lobule VI. Lobule VI was chosen as it has been shown to be functionally connected to posterior prefrontal cortex [Bernard et al., 2012]. We predicted that regions of the lateral posterior cerebellum would show connectivity patterns with the prefrontal cortex that parallel the rostral-caudal gradient of abstraction, suggesting that these lobules may subserve more specific components of EF.

In order to gain additional insight into the nature of CB-PFC network contributions to EF, we also examined task-based fMRI. Tasks in the HCP targeted a variety of functional domains including motor, language, working memory, relational processing, social processing, emotional processing, and gambling. These tasks were chosen to activate as many different functional network nodes as possible, in order to serve as seeds for connectivity analyses [Barch et al., 2013]. We chose four tasks that are reliable localizers for lateral prefrontal regions: the Relational Processing Task, the N-Back Working Memory Task, a Language Comprehension Task, and Motor Tapping.

The Relational Processing Task has been proposed as a localizer task for the RLPFC [Smith et al., 2007]. In this task, participants compared items on simple features (control condition) or determined if the same feature changed between two sets (i.e., relational condition). We predicted that the Relational Processing Task would activate the RLPFC and Crus I networks to a greater degree than the other tasks. The N-Back Task was embedded in a category representation task that has been shown to be a reliable localizer for the DLPFC [Barch et al., 2013; Drobyshevsky et al., 2006]. Therefore, we predicted that the Working Memory Task would activate the DLPFC and Crus II networks to a greater degree than the other tasks. The Language Comprehension Task involved comparing auditory stories with comprehension questions to math problems [Binder et al., 2011]. This task has been shown to activate inferior frontal and temporal regions associated with language processing. In the cerebellum, language tasks have been shown to activate both Crus I and Lobule VI [Stoodley et al., 2012; Stoodley and Schmahmann, 2009]. The Motor Mapping Task involved simple motor movements of the hands, toes, and tongue. We chose the right hand condition, which should activate the left premotor and motor cortices, and right cerebellar lobules IV-V and VIII [Stoodley et al., 2012].

A recent paper analyzed functional task activation in the cerebellum in these same tasks (using a less restricted set of HCP data), and found evidence for three distinct nonmotor representations [Guell et al., 2018a]. They found that working memory was associated with Crus I, Crus II, and Lobule VIIIb, language was associated with activation in Crus I and Crus II (more medial than the working memory activation), and right hand tapping activation was associated with Right Lobules V-VI and VIII. In their main manuscript they state that the relational processing task did not yield

sufficient activation, but in their supplementary materials they report a sub-threshold activation map for the relational processing task; this revealed that the relation vs. control match comparison was associated with similar activation as the working memory task.

Critically, Guell and colleagues [2018a] took a different approach than the current work. First, they only examined cerebellar task activation. Our goal was to identify dissociable cerebellar-PFC networks, while the goal of Guell and colleagues was to identify a functional topography in the cerebellar. Second, Guell and colleagues included participants irrespective of education, drug use history, and personal and family mental health history, while we selected "clean" controls with high levels of education, no history of drug use, and no personal or family mental health history. Third, we only chose unrelated individuals, as including related individuals violates statistical assumptions of independence [Winkler et al., 2014]. Lastly, Guell and colleagues [2018a] did not perform a group-level GLM, rather they calculated Cohen's d based on the average contrast maps, and chose a threshold of Cohen's d > 0.5. We performed a statistically conservative GLM using permutation methods, and for task-based activation, used grayordinate data (representing cortical data as a surface and subcortical/cerebellar data as a volume) which shows better cortical localization [Coalson et al., 2018].

Methods

Participants – HCP

Structural, resting-state fMRI (rfMRI), and cognitive task fMRI (tfMRI) data from the S900 Release of Human Connectome Project (WU-UMN HCP Consortium) were used in this investigation. The goal of recruitment in the WU-UMN HCP

Consortium was to capture a broad range of variability in healthy individuals with respect to behavioral, ethnic, and socioeconomic diversity [Van Essen et al., 2012]. Lifestyle and demographic data were collected alongside the imaging data and were used in this study to select for a sample meant to be representative of unrelated, non-clinical individuals across a variety of socioeconomic, behavioral, and ethnic backgrounds in order to maintain generalizability and control for any potential structural and functional similarities and differences linked to the factors above. Detailed descriptions of each variable used to eliminate participants are available here: https://wiki.humanconnectome.org (see HCP Data Dictionary Public- Updated for the 1200 Subject Release). To establish an ideal picture of CB-PFC network functioning without the influence of potential drug or disease confounds, we only selected data from unrelated individuals who psychologically and neurologically "clean": right-handed, high-school graduate or greater, no family history of mental illness, and no alcohol or drug abuse. More specifically, data were considered for this study only if the participant displayed right-handedness (Handedness>24), attained a high school degree (SSAGA_Educ>11), reported no family history of mental illness (FamHist_*_None = 1), did not meet the DSM4 criteria for Alcohol Abuse or Dependence (SSAGA_Alc_D4_Ab_Dx != 5; SSAGA_Alc_D4_Dp_Dx != 5), and did not meet the DSM criteria for Marijuana Dependence (SSAGA_Mj_Ab_Dep = 0). Data was further excluded if the participant reported more than 7 drinks per week for a female or 14 drinks per week for a male ([F]Total_Drinks_7days <8 OR [M]Total_Drinks_7days <15). Only one randomly selected participant from each family unit was used in order to account for any potential similarities in brain structure and function [Ganjgahi et al., 2015; Glahn et al., 2007; Pagliaccio et al., 2015; Thompson et al., 2001]. These

exclusions resulted in a sample size of 225 individuals ranging in age from 22 to 36 years (92 males, 133 females; see Supplemental Material for a list of participants included).

HCP image acquisition and preprocessing

Details on data acquisition in the HCP sample are reported by Van Essen and colleagues [2012]. rfMRI data for each participant consisted of 2, 15-minute scans (1200 volumes, 720 ms TR, 2 mm isotropic voxels); although the HCP database includes up to 4 rfMRI scans per each participant with 2 pairs of scans collected on different days, we selected only one pair of scans primarily to restrict demands on data storage, but also to avoid any potential fluctuations in cognitive state across the different days [Poldrack et al., 2015]. rfMRI data came from the Resting State fMRI 1 FIX-Denoised (Extended) Package which included preprocessed volumetric timeseries data that had been denoised using the FIX ICA-based automated method and registered with Multimodal Surface Matching-Folding (MSMsulc), a technique that results in superior registration of functional and structural data using cortical folding [Robinson et al., 2014]. Additional details on this pipeline are discussed in detail elsewhere [Glasser et al., 2013]. Note, that the data resulting from the HCP preprocessing was not smoothed, and any smoothing described below was on denoised, but unsmoothed data.

tfMRI data for each participant consisted of cross-run analyzed grayordinates data, a format that represents gray matter locations by cortical surface vertices or subcortical volume voxels. tfMRI data had undergone preprocessing with the *fMRISurface* pipeline [Glasser et al., 2013], registration using the advanced MSMall method (which utilizes cortical folding and function to align data), and were then analyzed via GLM through the first-level (individual run level) and second-level (across

runs, within subject) with the HCP Task fMRI Analysis Pipeline [Barch et al., 2013]. The grayordinates-based analysis is similar to a traditional volume-based analysis, with a GLM implemented in FSL using autocorrelation correction [Woolrich et al., 2001], however, spatial smoothing was done on the left and right hemisphere surfaces using a geodesic Gaussian algorithm. Subcortical gray matter time series were smoothed within defined gray matter parcels. Smoothing by 2 mm FWHM was done by the HCP *fMRISurface* Pipeline, and an additional smoothing was done in subsequent analyses to bring the total smoothing to 4 mm FWHM.

In addition to functional data, preprocessed T1 structural data were also downloaded for each participant. Structural scans had undergone gradient distortion correction, bias field correction, and registration to the 0.8 mm resolution MNI brain using MSMsulc. Structural images were used for tissue type segmentation for purposes of rfMRI data processing (see below).

Data analysis

Resting-state Functional Connectivity Analysis

rfMRI data underwent all additional processing and analysis using the CONN toolbox [v. 17e; Whitfield-Gabrieli and Nieto Castañón, 2012], a Matlab-based application designed for functional connectivity analysis. CONN was compiled as a standalone application for MATALB R2016b in centOS 6 running on a 128-core Intel Xeon Broadwell blade cluster. Preprocessing in CONN consisted of structural segmentation, smoothing (6mm FWHM), and artifact detection (global signal z-value threshold: 5, subject motion threshold: 0.9 mm). Data were then denoised with linear regression with confound regressors for 5 temporal components each from the segmented CSF and white matter, 24 motion realignment parameters, signal and/or

motion outliers, a linear trend regressor, and the 1st order derivative from the effect of rest. Although the data had already been denoised using ICA, we took an aggressive approach towards denoising and included the motion parameters (determined before ICA) in this regression. Finally, data underwent bandpass filtering (0.01 – 0.1 Hz).

Functional connectivity from Left and Right Crus I, Crus II, and Lobule VI to the rest of the brain was examined using a General Linear Model. ROIs were defined from the SUIT probabilistic cerebellum atlas [Diedrichsen et al., 2009]. The location of these ROIs are shown in Figure 8. The average BOLD signal timeseries was extracted from each ROI. At the first-level, a standard GLM was performed where the canonical hemodynamic response function was convolved with the rest condition. A semi-partial correlation approach was used, where all 6 ROIs were entered into one model to estimate their unique contributions. At the group-level, βs were saved as Fisher-transformed correlation coefficients. The connectivity of each ROI was considered against the other two ROIs in pairwise contrasts, e.g., Crus I > Lobule VI was coded as [1, 0, -1]. Thus, 6 contrasts were defined: Crus I > Crus II, Crus I > Lobule VI, Crus II > Crus I, Crus II > Lobule VI, Lobule VI > Crus I, Lobule VI > Crus II. Statistical maps were thresholded non-parametrically using a conservative thresholding approach, given the very large sample size; the cluster defining threshold was set to an FDR-corrected $p < .001$, and the resulting clusters were thresholded to a cluster-mass FDR-corrected $p < .001$ with 10,000 permutations. To better illustrate the patterns of connectivity for each ROI relative to the other two, we generated conjunction maps for each ROI e.g., (Crus I > Crus II) Λ (Crus I > Lobule VI). This was accomplished by creating binary masks of the corrected contrast maps and multiplying the two appropriate masks together. Cluster tables were generated using FSL's *autoaq*, a tool which performs automatic atlas

queries for the center of mass for each cluster. We used the Harvard-Oxford Cortical and Subcortical Atlases, and for prefrontal clusters, we used the Sallet Dorsal Frontal Atlas [Sallet et al., 2013] and the Neubert Ventral Frontal Atlas [Neubert et al., 2014]. As these atlases were only available for the right hemisphere, to label left hemisphere clusters we flipped the statistical maps along the x-axis. The volumetric thresholded results were mapped to the cortical surface to allow for better comparison with the task fMRI analyses. The Connectome Workbench (v. 1.3.1; https://www.humanconnectome.org/software/connectome-workbench) was used to map the volumes to the HCP S1200 Group Average Inflated Surface [Van Essen et al., 2017].

Task fMRI Group Analysis

As mentioned above, tfMRI data were downloaded in a pre-analyzed format, which consisted of cross-run analyzed dense grayordinates data smoothed to 4mm. Contrast Parameter Estimate (COPE) images from each participant were selected from each task for inclusion in group-level analyses. For the relational processing task, we chose the contrast for Relational > Match; for the working memory task, we chose the contrast for 2-back > 0-back; for the language task, we chose the contrast for Story > Math; and for the motor task we chose the contrast for Right Hand > Average. Data were analyzed with the Connectome Workbench. Analysis scripts are available at {create repository}. For each task, the COPE maps from each participant were merged and the merged files were then separated into volumetric data for subcortical areas and surface data for the left and right hemispheres, resulting in three maps for each task. For the left and right hemispheres, the midthickness surface mesh was used so that the adjacency (neighborhood) information between vertices can be computed. Group means for each

task were then analyzed using non-parametric permutation testing in PALM [Winkler et al., 2014] with 5000 permutations for each test. Clusters were identified with Threshold Free Cluster Enhancement (TFCE) [Smith and Nichols, 2009] with FWE-corrected p-values, stored as $-log(p)$ values to increase the spread of volumes for viewing purposes. Because 3 tests (left and right hemisphere surface and subcortical volume) were run for each of the four tasks, we set a minimum threshold of $-log(p) = 2.38$ which is equivalent to .004166 or .05/12. As this threshold produced large areas of overlap, and we wanted to identify unique clusters of activation, we further thresholded the maps at the 95th percentile of the t-values. As there are currently no tools available to create cluster tables in Connectome Workbench, we identified the location of activation clusters by overlaying the results on the label file of the Glasser et al. [2016] Multi-Modal Parcellation of 180 cortical areas. We placed a vertex in the center of each cluster of activation, and for large clusters that covered multiple areas, a vertex was placed in each area covered by the activation. The results (including the Multi-Modal Parcellation label file) are available on the Brain Analysis Library of Spatial Maps and Atlases (BALSA; https://balsa.wustl.edu/study/show/k53g) and on the Open Science Framework (https://osf.io/3vka4). Analysis scripts for the task fMRI analyses are also available on the Open Science Framework.

Results

Resting-State Functional Connectivity Results

Crus I

Connectivity from each ROI to the rest of the brain was contrasted with the other ROIs. Examining the conjunction of the contrasts of Crus I > Crus II and Crus I > Lobule VI, Crus I showed greater connectivity with several prefrontal regions: the

RLPFC, the frontal operculum, the rostral cingulate, and the dorsal premotor cortex (see Figure 1 and Tables 1&2). There were some notable differences between the left and right cerebellar ROIs. While there were bilateral RLPFC clusters for left Crus I, only the left RLPFC showed connectivity with right Crus I. In addition, the frontal operculum connectivity was only present for right Crus I. We further explore these discrepancies
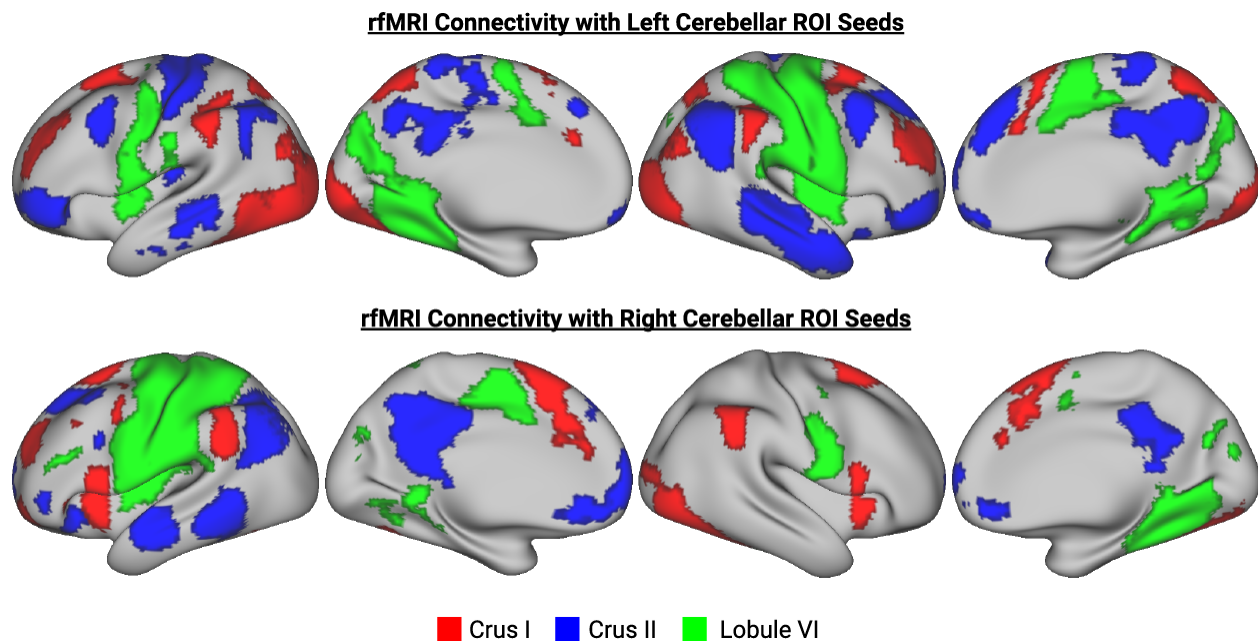

rfMRI Connectivity with Left Cerebellar ROI Seeds

rfMRI Connectivity with Right Cerebellar ROI Seeds

■ Crus I   ■ Crus II   ■ Lobule VI

Figure 1. Peak activations from the four functional tasks: working memory (red), relational processing (blue), language (green), and motor (yellow) overlaid on the inflated cortical surface (top row in each section) and the cerebellum (bottom row in each section). Cluster-corrected activation maps were further thresholded at the 95 percentile to isolate peaks of activation, and were binarized for display. The working memory activation was thresholded at T>10.98, relational processing was thresholded at T>9.34, language was thresholded at T>15.5, and motor was thresholded at T>13.45.

below.

In the RLPFC, Crus I connectivity was localized to area 46 and area 9/46d. While area 46 is often referred to as frontopolar area 10 [Gilbert et al., 2010; Leung et al., 2005], work has shown that this region differs from the more anterior area 10 in terms of its cytoarchitectonics [Bludau et al., 2013] as well as structural connectivity and functional coupling [Sallet et al., 2013]. Sallet and colleagues [2013] showed that area

46 shows maximal functional coupling with dorsal premotor cortex, rostral anterior cingulate, and inferior parietal lobule, while area 10 shows maximal coupling with ventromedial PFC and amygdala. As shown in Figures 2 & 3 (see also Supplemental Tables 1-4), the direct comparison of Crus I with each of the other two ROIs supported the results of the conjunction analysis. The main difference between the conjunction analyses and the direct comparison was the finding that the frontal operculum was only present in the comparison of Left Crus I and II, but not in the comparison of Left Crus I and Lobule VI. With the exception of the frontal operculum, the connectivity maps for the direct comparisons of left and right Crus I were more similar than suggested by the conjunction analyses. Overlaying the conjunction connectivity maps on the Yeo 17-area parcellation [Yeo et al., 2011] revealed that the RLPFC cluster, the rostral cingulate cluster, and the frontal operculum cluster were all part of the cingulo-opercular task control network, a network involved in stable task-level control and maintenance of goals [Dosenbach et al., 2008] (See Figure S1). Thus, as predicted, Crus I shows greater connectivity with regions of prefrontal cortex involved in higher-level abstract control compared to Crus II and Lobule VI.

Crus II

Turning to Crus II, the conjunction of Crus II > Crus I and Crus II > Lobule VI revealed two main areas of connectivity in the prefrontal cortex, one posterior DLPFC cluster, and one anterior ventrolateral PFC cluster (See Figure 1 and Tables 3 & 4). The posterior DLPFC cluster was located in areas 8A and ventral 9/46 in the left hemisphere and areas 8B, 9, and pre-SMA in the right hemisphere. The second area of connectivity was located in the Inferior Frontal Sulcus and area 47. Area 47 has been shown to exhibit functional coupling with nearby regions of anterior prefrontal cortex, precuneus,

as well as anterior lateral temporal cortex [Neubert et al., 2014]. Indeed, anterior lateral temporal cortex and precuneus were also connected with Crus II.

Examining Figure 1, the prefrontal connectivity was not as clear for the Right Crus II conjunction compared to the Left Crus II conjunction. Therefore, we examined the direct comparisons of Crus II to Crus I and Lobule VI to help clarify the patterns of connectivity. As shown in Figure 2, Left Crus II showed stronger connectivity compared to Crus I and Lobule VI in bilateral posterior DLPFC, bilateral anterior ventrolateral PFC, and medial area 9 (see also Supplemental Tables 5 & 7). When examining the connectivity of Right Crus II, Figure 3 illustrates that the comparison of Right Crus II and Lobule VI shows similar patterns of connectivity as the Left Crus II conjunction, but Right Crus II showed greater connectivity compared to Right Crus I in a cluster in the middle DLPFC, in between the posterior DLPFC and anterior ventrolateral PFC clusters (see also Supplemental Tables 6 & 8). This middle DLPFC cluster more closely resembles the predicted region of connectivity with Crus II, extending the length of ventral 9/46 [Petrides and Pandya, 1994], a region implicated in working memory function in humans and macaques [Petrides, 2005].

Lobule VI

As shown in Figure 1, there was little prefrontal connectivity with Left Lobule VI, with the bulk of connectivity located in the sensorimotor cortex. The conjunction for Right Lobule VI, however, showed a small cluster of connectivity in the left DLPFC. Turning to the direct comparison of Lobule VI and Crus I, there was no prefrontal connectivity for Left Lobule VI, but Right Lobule VI was more connected with the left DLPFC than Right Crus I (See Figures 2&3, Supplemental Tables 9-12). Comparing Lobule VI and Crus II, for the left and right ROIs there was connectivity with bilateral

anterior DLPFC (areas 46 and dorsal 9/46). This area of connectivity was slightly caudal to the RLPFC cluster connected with Crus I. This finding was somewhat surprising, and contrary to our predictions, as Lobule VI connectivity patterns at rest have implicated premotor cortical regions [Bernard et al., 2012]. However, task-based activation patterns do suggest contributions to higher-order processing [E et al., 2012; Guell et al., 2018b; Stoodley et al., 2012; Stoodley and Schmahmann, 2009]. Further, in their investigation of cerebellar sensorimotor networks, Kipping and colleagues [2013] demonstrated a similar pattern of connectivity, implicating the lateral prefrontal cortex.

Functional Connectivity Interim Summary

Comparisons across Crus I, Crus II, and Lobule VI suggest that their patterns of connectivity vary across the prefrontal cortex in a manner suggesting parallel PFC and cerebellar functional processing gradients. Crus I is most strongly associated with prefrontal cortical regions associated with higher level control, while Crus II was associated with areas implicated in working memory and more specific cognitive processes (as opposed to more abstract processing). Finally, Lobule VI was also

Figure 2. Comparison of resting-state connectivity for left cerebellar seeds. Seeds were derived from the SUIT Probabilistic Cerebellar Atlas and included Crus I, Crus II, and Lobule VI. Pairwise comparisons for seed-to-voxel connectivity were created with linear contrasts in CONN that included all three seeds and setting the weight for the third seed that was not of interest to 0, e.g., for the contrast of Left Crus I > Left Crus II, the weight for Left Lobule VI was set to 0, i.e., [1 -1 0].

correlated with many of these working memory regions, and somewhat surprisingly, there was no unique connectivity with areas associated with the planning of motoric responses, counter to our predictions.
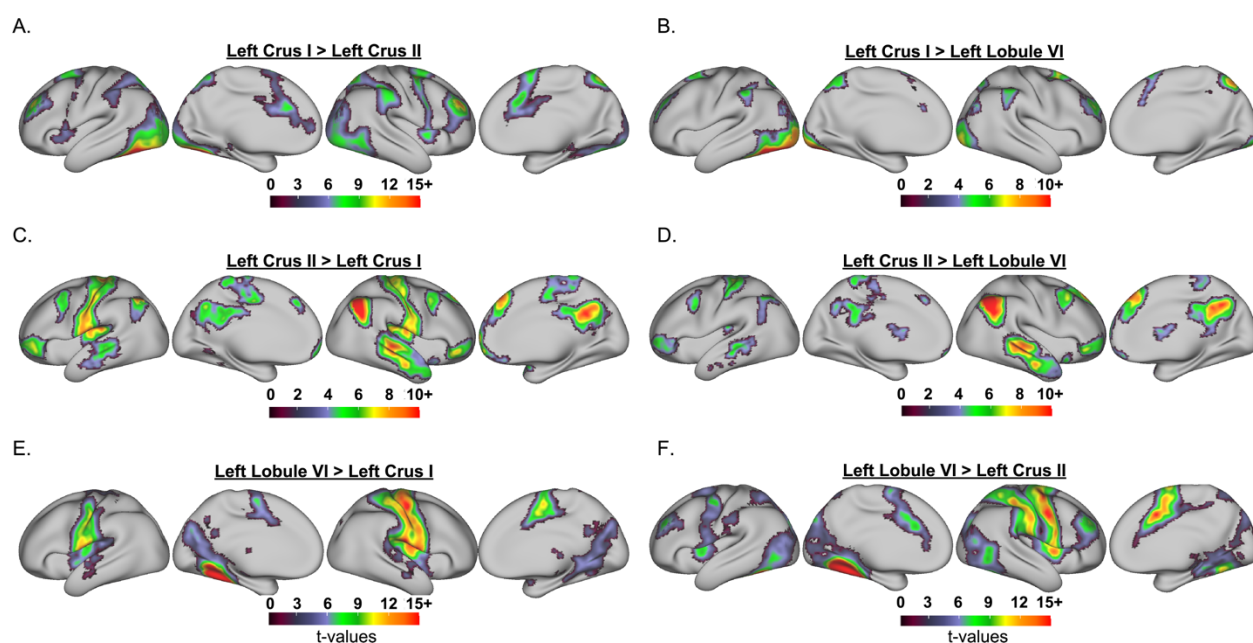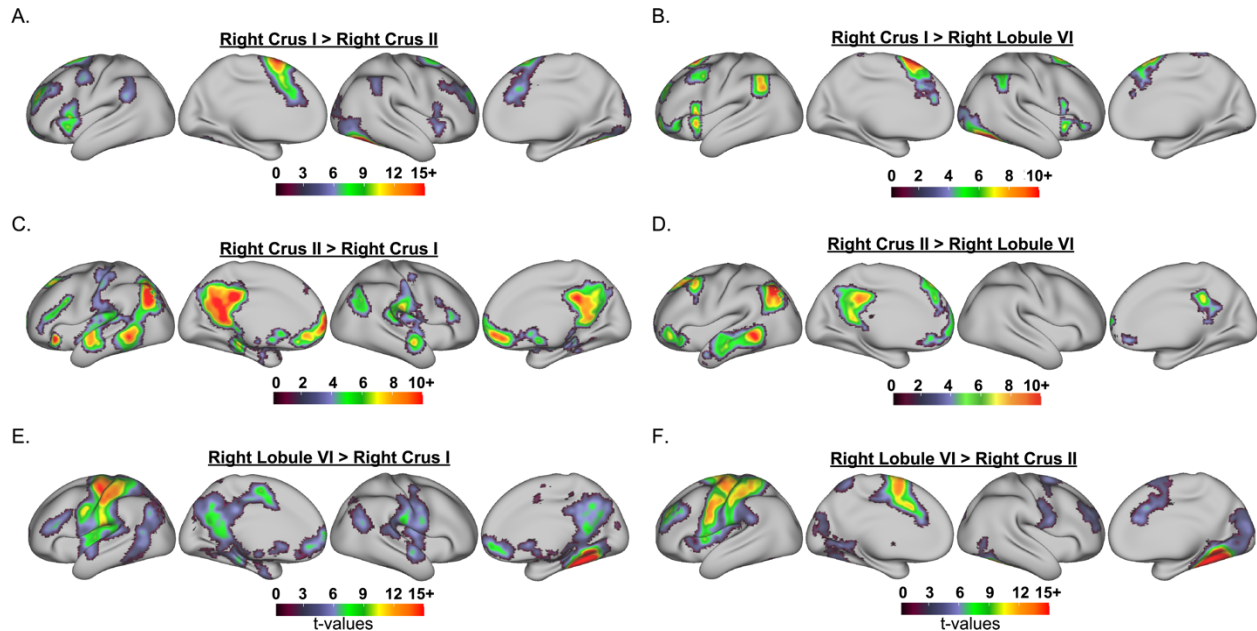

Figure 3. Comparison of resting-state connectivity for right cerebellar seeds. Seeds were derived from the SUIT Probabilistic Cerebellar Atlas and included Crus I, Crus II, and Lobule VI. Pairwise comparisons for seed-to-voxel connectivity were created with linear contrasts in CONN that included all three seeds and setting the weight for the third seed that was not of interest to 0, e.g., for the contrast of Right Crus I > Right Crus II, the weight for Right Lobule VI was set to 0, i.e., [1 -1 0].

Task-Based Functional Activation Results

Relational Processing Task

For the relational processing task, we examined activation for the Relational vs. Match contrast. This task has been suggested to serve as a localizer for RLPFC/ area 10 [Smith et al., 2007]. While we did observe rostral prefrontal activation, the activation was ventral to the expected area 10, in anterior 47r (See Figure 4 and Table 7). This cluster is similar to that which showed connectivity with Crus II, further differentiating these findings from our predictions. Additional prefrontal activation was found in the

Figure 4. Relational processing related cortical surface activation (left) and cerebellar volumetric activation (right). Results come from a group-level analysis of the contrast of relational vs. match for the Relational Processing Task.

anterior insula, posterior DLPFC, dorsal medial prefrontal cortex (area 8), and dorsal premotor cortex. In the cerebellum, there was activation of both Crus I and Crus II, as well as Lobule VI and Lobule VIIb. Smith and colleagues [2007] demonstrated that the Relational Processing Task robustly activates the RLPFC (i.e., the lateral portion of BA10) across participants, however, they did not report cluster coordinates for the group average, only reporting activation foci in BA10 for each participant. Nevertheless, for most participants, activation foci were located in the Superior and Middle Frontal Gyri, while area 47 is located in the Inferior Frontal Gyrus. In their multimodal cortical parcellation using the HCP data, Glasser and colleagues also found that area 47r was active in the Relational vs. Match contrast [Glasser et al., 2016; see Figure 23 of their Supplementary Neuroanatomical Results].

Working Memory Task

To assess brain activity associated with working memory, we used the 2-back vs. 0-back contrast from the embedded n-back task. Both the RLPFC and DLPFC were activated in this contrast, as shown in Figure 5 (see also Table 8). The RLPFC activity

was located in left area 9/46d and right area 10p. This area of activation was similar to the location that showed functional connectivity with Crus I. As shown in Figure 8, the DLPFC activation overlapped with the activation from the Relational Processing Task, suggesting this region serves a similar purpose in both tasks, likely working memory. There was also prefrontal activation in the dorsal premotor cortex and dorsal medial prefrontal cortex, largely overlapping with the Relational Processing Task activation. In the cerebellum, there was widespread activation, with Crus I and Crus II both activated, as well as Lobules I-V, V, VIIIb, and IX.
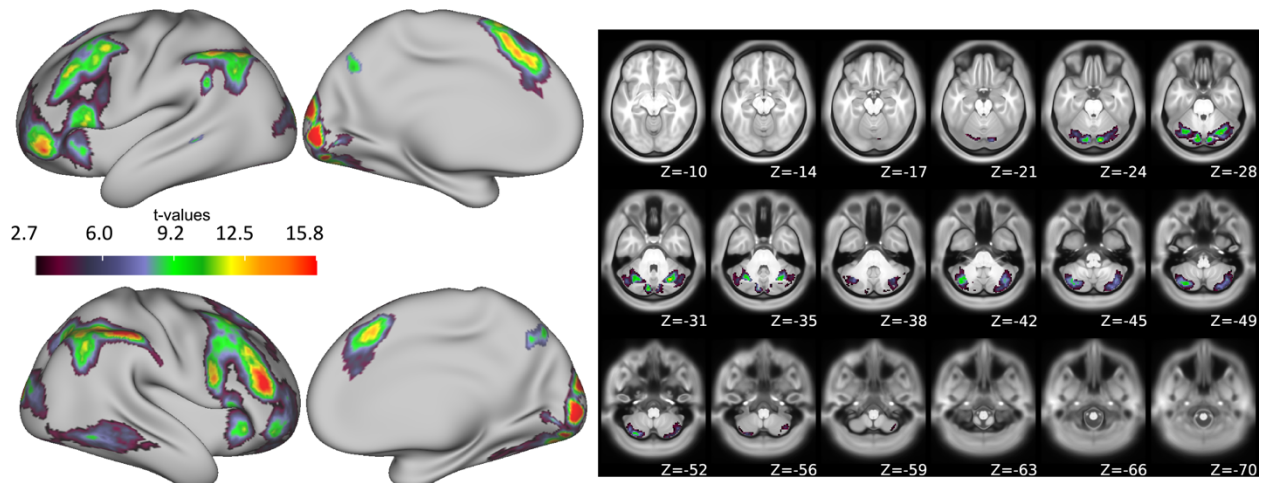

Figure 5. Working memory related cortical surface activation (left) and cerebellar volumetric activation (right). Results come from a group-level analysis of the contrast of 2-back vs. 0-back trials for the N-Back Task.

Language Task

To assess language processing, we used the Story vs. Math contrast. This contrast activated both the left and right posterior inferior frontal cortex (areas 45 and 47 lateral), the medial frontal pole, ventral area 8A, and the left Superior Frontal Language Area (see Figure 6 and Table 9). Unlike the other 3 tasks, language activated large areas of the temporal cortex, specifically, bilateral anterior temporal cortex and temporal parietal junction. In the cerebellum, bilateral Crus II and Lobule XI were activated, with

the Crus II peak activation being more lateral to that of the Relational Processing Task, as shown in Figure 8.

Figure 6. Language related cortical surface activation (left) and cerebellar volumetric activation (right). Results come from a group-level analysis of the contrast of story vs. math trials in the Story Task.

Motor Task

To assess motor function, we used the Right Hand contrast. Unsurprisingly, this was associated with left sensorimotor cortex and premotor cortex, as shown in Figure 7 and Table 10. In the cerebellum, Right Lobules VIIIb and V were activated.

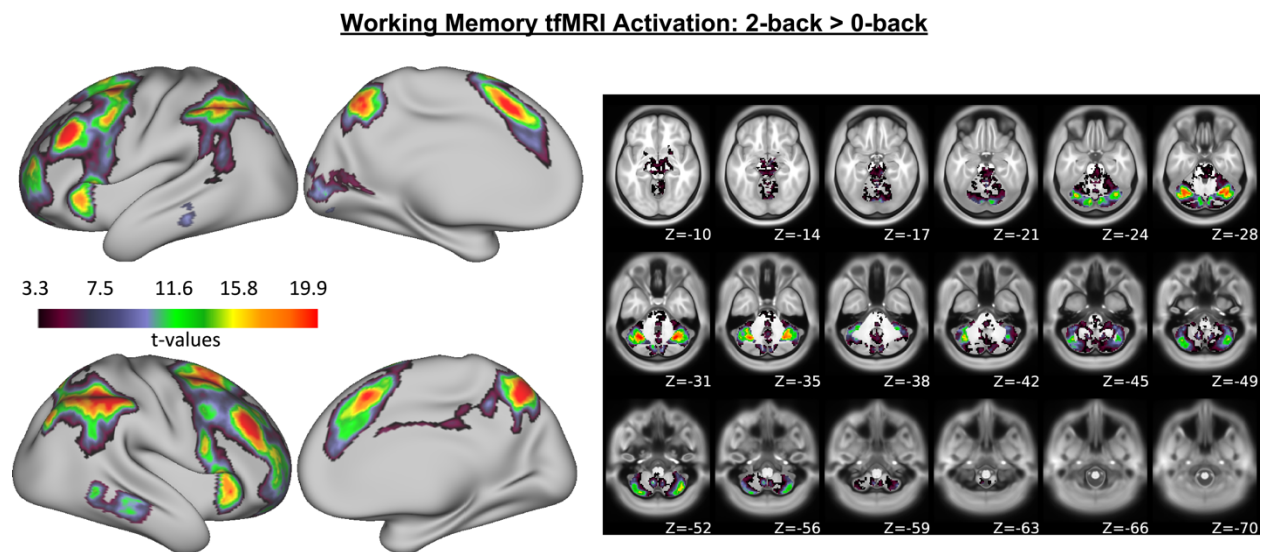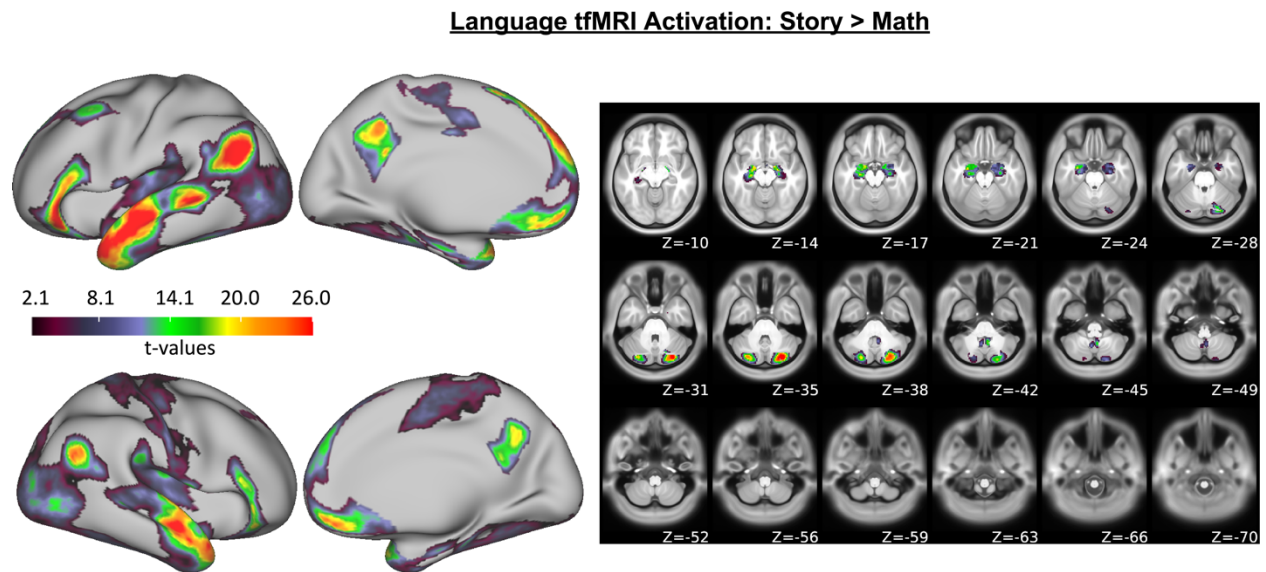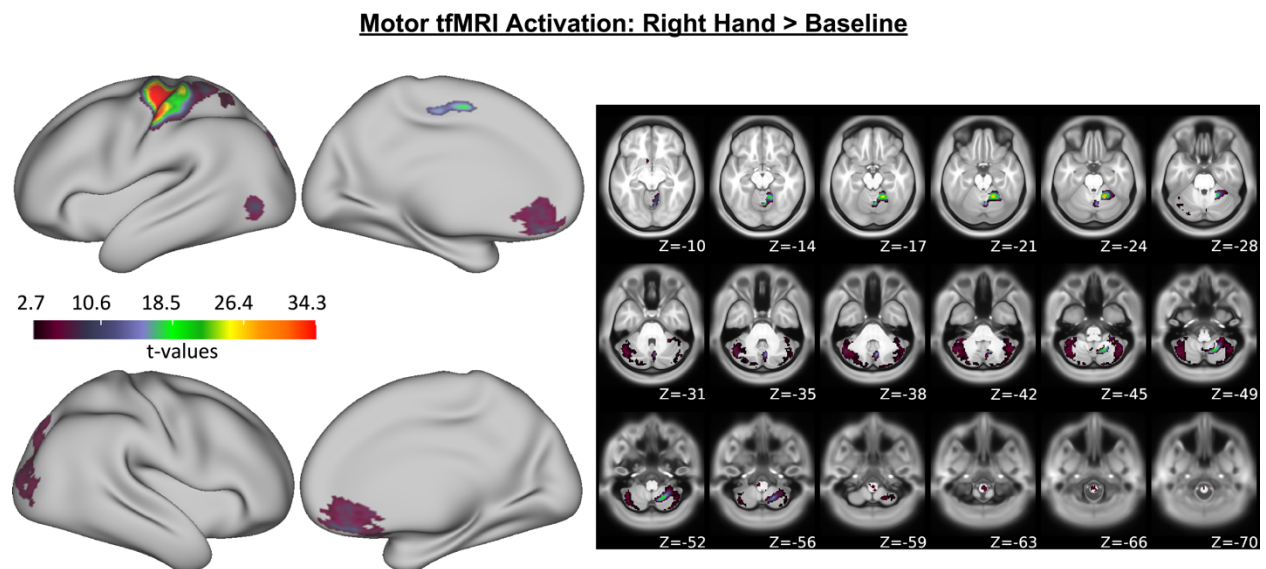*Figure 7.* Motor related cortical surface activation (left) and cerebellar volumetric activation (right). Results come from a group-level analysis of the contrast of right hand vs. baseline trials in the Motor Tapping Task.

Task-Related Activation Interim Summary

The analysis of task-related functional activation provided further evidence for existence of functional gradients of CB-PFC networks. As shown in Figure 8, there were dissociable areas of activation for all four tasks in the prefrontal cortex and cerebellum. There were overlapping areas of activation for the relational processing task and working memory task in the mid- and posterior DLPFC. In the cerebellum, these tasks showed overlapping areas of activation in both Crus I and Crus II, but the activation for the relational processing task was more posterior to that of the working memory task. However, there were some notable deviations from our predictions. As shown in Figure 8, in the RLPFC, the activation for the relational processing task and working memory task were reversed from what we predicted, with relational processing being more ventral, in a region connected more with Crus II than Crus I (see Figure 1). In addition, the relational processing task activated Crus II to a greater extent than the working memory task.
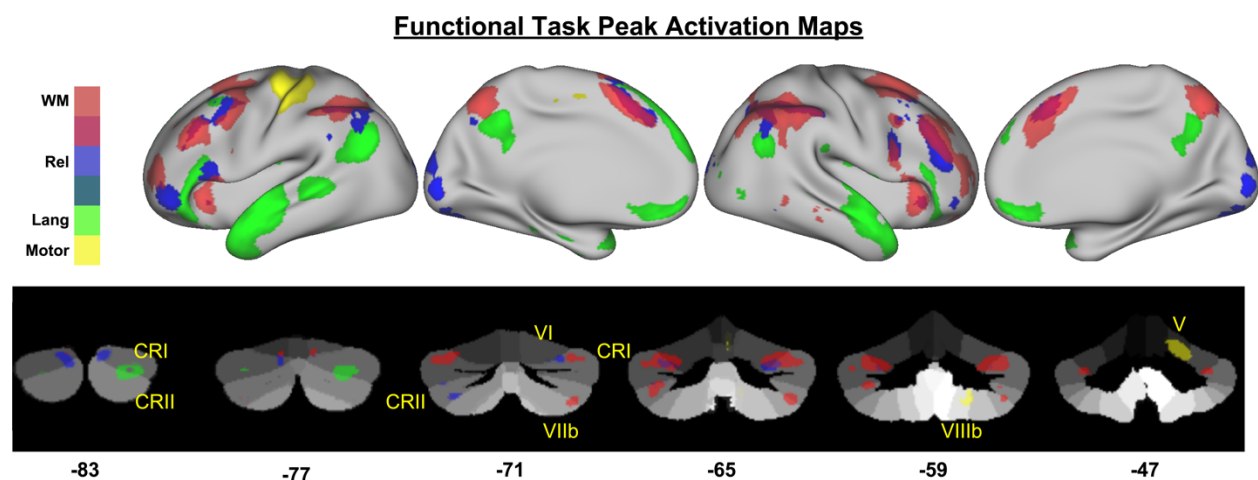
Figure 8. Peak activations from the four functional tasks: working memory (red), relational processing (blue), language (green), and motor (yellow) overlaid on the inflated cortical surface (top row in each section) and the cerebellum (bottom row in each section). Cluster-corrected activation maps were further thresholded at the 95 percentile to isolate peaks of activation, and were binarized for display. The working memory activation was thresholded at T>10.98, relational processing was thresholded at T>9.34, language was thresholded at T>15.5, and motor was thresholded at T>13.45.

Discussion

The goal of this study was to test the hypothesis that cerebellar-prefrontal connections are organized along a gradient. Across several domains, it has been demonstrated that the lateral prefrontal cortex is organized along a rostral-caudal gradient of abstraction, with anterior PFC associated with the most abstract levels of processing (e.g., long-term goals and integrating information across time levels) and posterior PFC associated with concrete information such as stimuli and responses. While previous work has demonstrated the possibility of a similar gradient in the basal ganglia [Nee and Brown, 2013; Verstynen et al., 2012], it is unclear if the cerebellum follows a similar gradient. Previous work has suggested that there is a functional topography for nonmotor tasks in the cerebellum [E et al., 2012; Guell et al., 2018a; Guell et al., 2018b; Stoodley et al., 2012], yet, it is unclear whether the functional topography in the cerebellum shows an abstraction gradient.

While the current study was limited in that we relied on tfMRI from tasks not necessarily optimized to investigate this purported functional gradient, the findings suggest that such a gradient of abstraction may be present in the cerebellum. There is limited evidence from task-based fMRI to support this hypothesis, however. To our knowledge, previous studies of levels of abstraction in EF have not focused on the cerebellum. The cerebellum is frequently not imaged due to limitations in coverage with standard imaging protocols. Moreover, standard spatial smoothing kernels employed in most cortical/whole-brain fMRI preprocessing pipelines (e.g., 6-8 mm FWHM) may be too large to allow for the separation of neighboring lobules [Bernard et al., 2012; Bernard and Seidler, 2013]. Nevertheless, the suggestion that such a functional gradient

exists in the cerebellum is supported by a number of previous studies [e.g., Balsters et al., 2013; Stoodley et al., 2012; Stoodley and Schmahmann, 2009].

We found that Crus I was connected to the RLPFC more strongly than Crus II and Lobule VI. This is in line with our prior work which investigated the connectivity of each cerebellar lobule, but did not compare the networks of different lobules [Bernard et al., 2012]. However, there was mixed evidence for our prediction that the Relational Processing Task would be associated with activation in both Crus I and RLPFC. While there was anterior PFC activation for the task, it was more ventral than the region typically referred to as RLPFC. Nevertheless, the Relational Processing Task did show activation in Crus I. There is evidence to suggest that Crus I is involved in higher-order cognitive processing, in concert with anterior prefrontal cortex. We have previously shown that Crus I and the rostral lateral prefrontal cortex are activated when participants perform voluntary task switching, a task that requires them to select tasks according to abstract, internally maintained task goals [Orr and Banich, 2014]. The rostral lateral prefrontal cortex has also been linked to prospective memory, i.e., remembering to perform an action after a delay [Burgess et al., 2003]. Several studies of prospective memory have shown activation of Crus I [Burgess et al., 2003; Reynolds et al., 2009]. Further, when examining individuals who don't show multitasking costs, aka "supertaskers", Medeiros-Ward and colleagues [2014] found that Crus I showed a group-by-load effect along with the rostral lateral prefrontal cortex.

While a number of studies have implicated a role of Crus I in executive function, there is less evidence for a role of Crus II. In an fMRI meta-analysis, Stoodley & Schmahmann [2009] found strong activation overlap in Crus II during language tasks. Similarly, here, in our own tfMRI analysis of language processing using HCP data, we

also found cerebellar activation in Crus II. The current connectivity findings also support a link between Crus II and language, as Crus II was connected with language-related regions of posterior inferior frontal gyrus, including areas 45 and 47. However, Buckner and colleagues [2011] identified a connection between Crus II and the default mode network. If the center of gravity of the Right Crus II seed (from the SUIT atlas thresholded at 50%, coordinates: 26, -76, -42) is entered into *neurosynth* [Yarkoni et al., 2011], top meta-analytic terms associated with the region include "past", "socially", and "autobiographical". Nevertheless, the functional connectivity and meta-analytic connectivity maps for the same region from *neurosynth* (http://neurosynth.org/locations/?y=-76&x=26&z=-42) contains left posterior inferior frontal gyrus cortex. Thus, while several lines of evidence support a role for Crus II in language, further studies are needed to clarify the nature of this role.

While we predicted that Lobule VI would should show connectivity with posterior prefrontal cortex, the connectivity was more posterior in primary motor cortex, rather than premotor cortex. Prior studies have demonstrated connectivity between Lobule VI and premotor cortex [Bernard et al., 2012], though Kipping and colleagues [2013] demonstrated associations with more lateral prefronal cortical regions. The conflicting results here may however be due to the nature of our analyses where we directly compared Lobule VI with Crus I and II. As seen in Figure 2, both Crus I and II also have areas of connectivity with dorsal and ventral pre-motor cortical regions, and thus it may be the case that the greater connectivity for Lobule VI is with more primary motor cortical regions. However, it is also notable that the sample here is at much higher resolution and has a significantly larger sample than prior work [Bernard et al., 2012]. Reineberg and Banich [2016] showed that individual difference in network dynamics at

rest in Lobule VI were associated with working memory updating. Further, meta-analytic evidence suggests that this region is involved not only in working memory, but across motor tasks and learning, and in language as well [E et al., 2012; Stoodley & Schmahmann, 2009; Bernard & Seidler, 2013]. The seemingly diverse roles and contributions of Lobule VI suggest that it is a transition area of sorts such that there is involvement in more abstract higher order thinking to some degree, but also makes contributions to motor planning. Because much of the evidence in this regard comes from meta-analysis, it is not feasible to dissociate the more concrete motor-reliant execution aspects of these tasks from the more abstract processing. However, the stronger resting state associations with motor cortical regions that that we see with Lobule VI, particularly relative to Crus I and Crus II, suggest that perhaps the role of this cerebellar region is with respect to the more concrete aspects of motor response selection during the performance of higher order cognitive tasks. Future work specifically dissociating these levels of abstraction with respect to the cerebellum is clearly warranted in the future.

Here, using a large sample of individuals from the HCP, we carefully probed both the functional connectivity and activation of cerebellar lobules with respect to one another, as a first step towards understanding cerebellar contributions to executive function. While past work has taken a targeted lobular approach [Bernard et al., 2012], looked at the cerebellum more generally [Habas and Cabanis, 2007; O'Reilly et al., 2010], or made comparisons framed by the prefrontal cortex broadly defined [Krienen & Buckner, 2009], this cerebellar approach allows us to carefully interrogate connectivity patterns that are of potential importance to our understanding of EF. Broadly speaking, our results suggest that a gradient of abstraction may also be present in the cerebellum,

paralleling what is see in the PFC [e.g., Badre, 2008], likely subserved by the closed-loop circuitry linking these two disparate brain regions [Bernard et al., 2016; Kelly and Strick, 2003; Salmi et al., 2010; Strick et al., 2009]. While the exact role of the cerebellum in non-motor behavior remains unknown, it has been suggested that the structure acts to process internal models of thought [Ramnani, 2006; Ito, 2008; Ramnani, 2014], much as is done in the motor domain [e.g., Imamizu et al., 2000]. Across cerebellar lobules, the cytoarchitectonics remain the same, only the cortical connections change, suggesting a similar computation is being performed, just on distinct inputs [Ramnani, 2006; Ito, 2008; Ramnani, 2014]. In his more recent writings on this topic, Ramnani [2014] has suggested that the cerebellum supports more automated processes after learning, as compared to the more cognitively demanding top-down processes that occur early on when performing a task. With damage and disease, one would therefore experience deficits in thought and processing, such as those seen in patients with schizophrenia [Andreasen et al., 1996; Andreasen et al., 1998], or those with cerebellar infarct [Schmahmann and Sherman, 1998].

Given the complex nature of EF, as well as its importance in the completion of activities of daily living, maintaining this domain is critically important. Here, the suggestion that the cerebellum engages with the PFC in a manner that parallels the gradient of abstraction in the PFC means that we now have additional areas of investigation for understanding EF, or its breakdown in the case of disease or infarct. Further, this provides additional targets of intervention and remediation to improve these skills in impacted populations. Future work targeting the relative contributions of the cerebellum, and ideally its lobular subregions, taking advantage of non-invasive

brain stimulation stand to provide important insights into the necessity of this region

for EF, and its underlying domains of function.

References

Alexander GE, DeLong MR, Strick PL (1986): Parallel organization of functionally segregated circuits linking basal ganglia and cortex. Annu Rev Neurosci 9:357–381.

Andreasen NC, O'Leary DS, Cizadlo T, Arndt S, Rezai K, Ponto LL, Watkins GL, Hichwa RD (1996): Schizophrenia and cognitive dysmetria: a positron-emission tomography study of dysfunctional prefrontal-thalamic-cerebellar circuitry. Proc Natl Acad Sci U S A 93:9985–90.

Andreasen NC, Paradiso S, O'Leary DS (1998): "Cognitive dysmetria" as an integrative theory of schizophrenia: a dysfunction in cortical-subcortical-cerebellar circuitry? Schizophr Bull 24:203–18.

Badre D (2008): Cognitive control, hierarchy, and the rostro-caudal organization of the frontal lobes. Trends Cogn Sci 12:193–200.

Balsters JH, Laird AR, Fox PT, Eickhoff SB (2014): Bridging the gap between functional and anatomical features of cortico-cerebellar circuits using meta-analytic connectivity modeling. Hum Brain Mapp 35:3152–3169.

Balsters JH, Whelan CD, Robertson IH, Ramnani N (2013): Cerebellum and cognition: Evidence for the encoding of higher order rules. Cereb Cortex 23:1433–43.

Banich MT (2009): Executive Function: The Search for an Integrated Account. Curr Dir Psychol Sci 18:89–94.

Barch DM, Burgess GC, Harms MP, Petersen SE, Schlaggar BL, Corbetta M, Glasser MF, Curtiss S, Dixit S, Feldt C, Nolan D, Bryant E, Hartley T, Footer O, Bjork JM, Poldrack RA, Smith SM, Johansen-Berg H, Snyder AZ, Van Essen DC (2013): Function in the human connectome: Task-fMRI and individual differences in behavior. Neuroimage 80:169–89.

Bernard JA, Orr JM, Mittal VA (2016): Differential motor and prefrontal cerebello-cortical network development: Evidence from multimodal neuroimaging. Neuroimage 124:591–601.

Bernard JA, Peltier SJ, Benson BL, Wiggins JL, Jaeggi SM, Buschkuehl M, Jonides J, Monk CS, Seidler RD (2014): Dissociable Functional Networks of the Human Dentate Nucleus. Cereb Cortex 24:2151–2159.

Bernard JA, Seidler RD (2013): Relationships Between Regional Cerebellar Volume and Sensorimotor and Cognitive Function in Young and Older Adults. Cerebellum 12:721–737.

Bernard JA, Seidler RD, Hassevoort KM, Benson BL, Welsh RC, Wiggins JL, Jaeggi SM, Buschkuehl M, Monk CS, Jonides J, Peltier SJ (2012): Resting state cortico-cerebellar functional connectivity networks: a comparison of anatomical and self-organizing map approaches. Front Neuroanat 6:31.

Binder JR, Gross WL, Allendorfer JB, Bonilha L, Chapin J, Edwards JC, Grabowski TJ, Langfitt JT, Loring DW, Lowe MJ, Koenig K, Morgan PS, Ojemann JG, Rorden C, Szaflarski JP, Tivarus ME, Weaver KE (2011): Mapping anterior temporal lobe language areas with fMRI: A multicenter normative study. Neuroimage 54:1465–1475.

Bludau S, Eickhoff SB, Mohlberg H, Caspers S, Laird AR, Fox PT, Schleicher A, Zilles K, Amunts K (2013): Cytoarchitecture, probability maps and functions of the human frontal pole. Neuroimage.

Buckner RL, Krienen FM, Castellanos A, Diaz JC, Yeo BTT (2011): The organization of the human cerebellum estimated by intrinsic functional connectivity. J Neurophysiol 106:2322–2345.

Burgess PW, Scott SK, Frith CD (2003): The role of the rostral frontal cortex (area 10) in prospective memory: a lateral versus medial dissociation. Neuropsychologia 41:906–918.

Burgess PW, Simons JS, Dumontheil I, Gilbert SJ (2007): The gateway hypothesis of rostral prefrontal cortex (area 10) function. Trends Cogn Sci 11:290–298.

Coalson TS, Van Essen DC, Glasser MF (2018): The impact of traditional neuroimaging methods on the spatial localization of cortical areas. Proc Natl Acad Sci 115:1–23.

Diedrichsen J, Balsters JH, Flavell J, Cussans E, Ramnani N (2009): A probabilistic MR atlas of the human cerebellum. Neuroimage 46:39–46.

Dosenbach NUF, Fair DA, Cohen AL, Schlaggar BL, Petersen SE (2008): A dual-networks architecture of top-down control. Trends Cogn Sci 12:99–105.

Drobyshevsky A, Baumann SB, Schneider W (2006): A rapid fMRI task battery for mapping of visual, motor, cognitive, and emotional function. Neuroimage 31:732–744.

Dum RP, Strick PL (2003): An unfolded map of the cerebellar dentate nucleus and its projections to the cerebral cortex. J Neurophysiol 89:634–639.

E K-H, Chen S-HA, Ho M-HR, Desmond JE (2012): A meta-analysis of cerebellar contributions to higher cognition from PET and fMRI studies. Hum Brain Mapp 000.

Van Essen DC, Smith J, Glasser MF, Elam J, Donahue CJ, Dierker DL, Reid EK, Coalson T, Harwell J (2017): The Brain Analysis Library of Spatial maps and Atlases (BALSA) database. Neuroimage 144:270–274.

Van Essen DC, Ugurbil K, Auerbach EJ, Barch DM, Behrens TEJ, Bucholz R, Chang A, Chen L, Corbetta M, Curtiss SW, Della Penna S, Feinberg DA, Glasser MF, Harel N,

Heath AC, Larson-Prior L, Marcus D, Michalareas G, Moeller S, Oostenveld R, Petersen SE, Prior F, Schlaggar BL, Smith SM, Snyder AZ, Xu J, Yacoub E (2012): The Human Connectome Project: A data acquisition perspective. Neuroimage 62:2222–2231.

Ganjgahi H, Winkler AM, Glahn DC, Blangero J, Kochunov P, Nichols TE (2015): Fast and powerful heritability inference for family-based neuroimaging studies. Neuroimage 115:256–268.

Gilbert SJ, Gonen-Yaacovi G, Benoit RG, Volle E, Burgess PW (2010): Distinct functional connectivity associated with lateral versus medial rostral prefrontal cortex: a meta-analysis. Neuroimage 53:1359–67.

Glahn DC, Thompson PM, Blangero J (2007): Neuroimaging endophenotypes: Strategies for finding genes influencing brain structure and function. Hum Brain Mapp 28:488–501.

Glasser MF, Coalson TS, Robinson EC, Hacker CD, Harwell J, Yacoub E, Ugurbil K, Andersson J, Beckmann CF, Jenkinson M, Smith SM, Van Essen DC (2016): A multi-modal parcellation of human cerebral cortex. Nature 536:171–178.

Glasser MF, Sotiropoulos SN, Wilson JA, Coalson TS, Fischl B, Andersson JLR, Xu J, Jbabdi S, Webster M, Polimeni JR, Van Essen DC, Jenkinson M (2013): The minimal preprocessing pipelines for the human connectome project. Neuroimage 80:105–124.

Guell X, Gabrieli JDE, Schmahmann JD (2018a): Triple representation of language, working memory, social and emotion processing in the cerebellum: convergent evidence from task and seed-based resting-state fMRI analyses in a single large cohort. Neuroimage 172:437–449.

Guell X, Schmahmann JD, Gabrieli J DE, Ghosh SS (2018b): Functional gradients of the cerebellum. Elife 7:1–22.

Habas C, Cabanis EA (2007): Anatomical parcellation of the brainstem and cerebellar white matter: a preliminary probabilistic tractography study at 3 T. Neuroradiology 49:849–63.

Imamizu H, Miyauchi S, Tamada T, Sasaki Y, Takino R, Pütz B, Yoshioka T, Kawato M (2000): Human cerebellar activity reflecting an acquired internal model of a new tool. Nature 403:192–195.

Ito M (2008): Control of mental activities by internal models in the cerebellum. Nat Rev Neurosci 9:304–313.

Kelly RM, Strick PL (2003): Cerebellar loops with motor cortex and prefrontal cortex of a nonhuman primate. J Neurosci 23:8432–8444.

Kerns JG, Nuechterlein KH, Braver TS, Barch DM (2008): Executive Functioning Component Mechanisms and Schizophrenia. Biol Psychiatry 64:26–33.

Kipping JA, Grodd W, Kumar V, Taubert M, Villringer A, Margulies DS (2013): Overlapping and parallel cerebello-cerebral networks contributing to sensorimotor control: An intrinsic functional connectivity study. Neuroimage 83:837–848.

Koechlin E, Hyafil A (2007): Anterior Prefrontal Function and the Limits of Human Decision-Making. Science (80-) 318:594–598.

Krienen FM, Buckner RL (2009): Segregated fronto-cerebellar circuits revealed by intrinsic functional connectivity. Cereb Cortex 19:2485–2497.

Leiner HC, Leiner AL, Dow RS (1993): Cognitive and language functions of the human cerebellum. Trends Neurosci 16:444–447.

Leiner HC, Leiner AL, Dow RS (1986): Does the cerebellum contribute to mental skills?

Behav Neurosci 100:443–454.

Leung H-C, Gore JC, Goldman-Rakic PS (2005): Differential Anterior Prefrontal Activation during the Recognition Stage of a Spatial Working Memory Task. Cereb Cortex 15:1742–1749.

Masterman DL, Cummings JL (1997): Frontal-subcortical circuits: the anatomic basis of executive, social and motivated behaviors. J Psychopharmacol 11:107–114.

Medeiros-Ward N, Watson JM, Strayer DL (2014): On supertaskers and the neural basis of efficient multitasking. Psychon Bull Rev September:1–8.

Miller EK, Cohen JD (2001): An integrative theory of prefrontal cortex function. Annu Rev Neurosci 24:167–202.

Nee DE, Brown JW (2013): Dissociable Frontal–Striatal and Frontal–Parietal Networks Involved in Updating Hierarchical Contexts in Working Memory. Cereb Cortex 23:2146–2158.

Neubert F-X, Mars RB, Thomas AG, Sallet J, Rushworth MFS (2014): Comparison of human ventral frontal cortex areas for cognitive control and language with areas in monkey frontal cortex. Neuron 81:700–13.

O'Reilly JX, Beckmann CF, Tomassini V, Ramnani N, Johansen-Berg H (2010): Distinct and overlapping functional zones in the cerebellum defined by resting state functional connectivity. Cereb Cortex 20:953–965.

O'Reilly RC (2010): The What and How of prefrontal cortical organization. Trends Neurosci 33:355–361.

Orr JM, Banich MT (2014): The neural mechanisms underlying internally and externally guided task selection. Neuroimage 84:191–205.

Pagliaccio D, Barch DM, Bogdan R, Wood PK, Lynskey MT, Heath AC, Agrawal A

(2015): Shared Predisposition in the Association Between Cannabis Use and Subcortical Brain Structure. JAMA Psychiatry 72:994.

Petrides M (2005): Lateral prefrontal cortex: architectonic and functional organization. Philos Trans R Soc Lond B Biol Sci 360:781–795.

Petrides M, Pandya DN (1994): Comparative architectonic analysis of the human and the macaque frontal cortex. In: Boller, F, Grafman, J, editors. Handbook of Neuropsychology. Amsterdam: Elsevier. pp 17–58.

Poldrack RA, Laumann TO, Koyejo O, Gregory B, Hover A, Chen MY, Gorgolewski KJ, Luci J, Joo SJ, Boyd RL, Hunicke-Smith S, Simpson ZB, Caven T, Sochat V, Shine JM, Gordon E, Snyder AZ, Adeyemo B, Petersen SE, Glahn DC, Mckay DR, Curran JE, Göring HHH, Carless MA, Blangero J, Dougherty R, Leemans A, Handwerker DA, Frick L, Marcotte EM, Mumford JA (2015): Long-term neural and physiological phenotyping of a single human. Nat Commun 6.

Ramnani N (2006): The primate cortico-cerebellar system: anatomy and function. Nat Rev Neurosci 7:511–522.

Ramnani N (2014): Automatic and Controlled Processing in the Corticocerebellar System. In: Ramnani, N, editor. Progress in Brain Research 1st ed. Elsevier B.V. Vol. 210, pp 255–285.

Reineberg AE, Banich MT (2016): Functional connectivity at rest is sensitive to individual differences in executive function: A network analysis. Hum Brain Mapp 37:2959–2975.

Reynolds JR, West R, Braver TS (2009): Distinct neural circuits support transient and sustained processes in prospective memory and working memory. Cereb Cortex 19:1208–1221.

Robinson EC, Jbabdi S, Glasser MF, Andersson J, Burgess GC, Harms MP, Smith SM, Van Essen DC, Jenkinson M (2014): MSM: A new flexible framework for multimodal surface matching. Neuroimage 100:414–426.

Sallet J, Mars RB, Noonan MP, Neubert F-X, Jbabdi S, O'Reilly JX, Filippini N, Thomas AG, Rushworth MFS (2013): The organization of dorsal frontal cortex in humans and macaques. J Neurosci 33:12255–12574.

Salmi J, Pallesen KJ, Neuvonen T, Brattico E, Korvenoja A, Salonen O, Carlson S (2010): Cognitive and Motor Loops of the Human Cerebro-cerebellar System. J Cogn Neurosci 22:2663–2676.

Sang L, Qin W, Liu Y, Han W, Zhang Y, Jiang T, Yu C (2012): Resting-state functional connectivity of the vermal and hemispheric subregions of the cerebellum with both the cerebral cortical networks and subcortical structures. Neuroimage 61:1213–1225.

Schmahmann JD, Sherman JC (1998): The cerebellar cognitive affective syndrome. Brain 121:561–579.

Smith R, Keramatian K, Christoff K (2007): Localizing the rostrolateral prefrontal cortex at the individual level. Neuroimage 36:1387–96.

Smith SM, Nichols TE (2009): Threshold-free cluster enhancement: addressing problems of smoothing, threshold dependence and localisation in cluster inference. Neuroimage 44:83–98.

Snyder HR (2013): Major depressive disorder is associated with broad impairments on neuropsychological measures of executive function: a meta-analysis and review. Psychol Bull 139:81–132.

Stoodley CJ, Schmahmann JD (2009): Functional topography in the human cerebellum:

a meta-analysis of neuroimaging studies. Neuroimage 44:489–501.

Stoodley CJ, Valera EM, Schmahmann JD (2012): Functional topography of the cerebellum for motor and cognitive tasks: An fMRI study. Neuroimage 59:1560–1570.

Strick PL, Dum RP, Fiez JA (2009): Cerebellum and Nonmotor Function. Annu Rev Neurosci 32:413–434.

Thompson PM, Cannon TD, Narr KL, van Erp T, Poutanen V-P, Huttunen M, Lönnqvist J, Standertskjöld-Nordenstam C-G, Kaprio J, Khaledy M, Dail R, Zoumalan CI, Toga AW (2001): Genetic influences on brain structure. Nat Neurosci 4:1253–1258.

Verstynen TD, Badre D, Jarbo K, Schneider W (2012): Microstructural organizational patterns in the human corticostriatal system. J Neurophysiol 107:2984–2995.

Volkow ND, Wang G-J, Fowler JS, Tomasi D, Telang F (2011): Addiction: beyond dopamine reward circuitry. Proc Natl Acad Sci U S A 108:15037–42.

Whitfield-Gabrieli S, Nieto Castañón A (2012): Conn: a functional connectivity toolbox for correlated and anticorrelated brain networks. Brain Connect 2:125–141.

Winkler AM, Ridgway GR, Webster M a, Smith SM, Nichols TE (2014): Permutation Inference for the General Linear Model. Neuroimage 92:381–97.

Woolrich MW, Ripley BD, Brady M, Smith SM (2001): Temporal Autocorrelation in Univariate Linear Modeling of FMRI Data. Neuroimage 14:1370–1386.

Yarkoni T, Poldrack RA, Nichols TE, Van Essen DC, Wager TD (2011): Large-scale automated synthesis of human functional neuroimaging data. Nat Methods 8:665–675.

Yeo BTT, Krienen FM, Sepulcre J, Sabuncu MR, Lashkari D, Hollinshead M, Roffman JL, Smoller JW, Zöllei L, Polimeni JR, Fischl B, Liu H, Buckner RL (2011): The

organization of the human cerebral cortex estimated by intrinsic functional

connectivity. J Neurophysiol 106:1125–65.

Tables

Table 1. Atlas query of conjunction of Left Crus I connectivity results. For large clusters, sub-region labels are listed below. COG: Center of Gravity.

Cluster Index	Voxels	COG X (mm)	COG Y (mm)	COG Z (mm)	COG Label
10	10476	-17.4	-79.5	-13.9	42% Occipital Fusiform Gyrus
9	2175	10.2	-68.8	51.5	42% Precuneous Cortex
8	865	15.2	15.3	59.6	47% PreSMA
7	619	-20.5	10.1	62.4	45% Ant PMd
6	596	41.6	-47.5	-44.2	73% Right Crus II
5	544	-49.7	-42.5	46.4	40% Supramarginal Gyrus
4	538	31.6	50.9	29	51% Area 46
3	520	-28.4	48.2	29	61% Area 9/46D
2	495	51.7	-39.6	44.1	52% Supramarginal Gyrus
1	27	12.5	-102	16.7	51% Occipital Pole

Structures to which each cluster belongs to:

Cluster #10	Average Atlas Probability Within Cluster
Lateral Occipital Cortex, inferior division	10.4
Occipital Fusiform Gyrus	4.9
Occipital Pole	15.2

Cluster #9	Average Atlas Probability Within Cluster
Lateral Occipital Cortex, superior division	40.8
Precuneous Cortex	11.3

Cluster #8	Average Atlas Probability Within Cluster
Supplementary Motor Area	9.9
Pre-Supplementary Motor Area	8.5
Area 8A	10.6
Anterior Premotor Dorsal (PMd)	13.6

Cluster #7	Average Atlas Probability Within Cluster
Pre-Supplementary Motor Area	7.0
Anterior Premotor Dorsal (PMd)	29.6

Cluster #6	Average Atlas Probability Within Cluster
Right Crus I	22.0
Right Crus II	22.3
Right VIIb	14.1

Cluster #5	Average Atlas Probability Within Cluster
Supramarginal Gyrus, anterior division	19.8
Supramarginal Gyrus, posterior division	28.1

Cluster #4	Average Atlas Probability Within Cluster
Area 9/46D	20.9
Area 46	18.0

Cluster #3	Average Atlas Probability Within Cluster
Area 9/46D	29.0
Area 46	26.6
Area 8B	7.9

Table 2. Atlas query of conjunction of Right Crus I connectivity results. For large clusters, sub-region labels are listed below. COG: Center of Gravity.

ClusterIndex	Voxels	COG X (mm)	COG Y (mm)	COG Z (mm)	COG Label
12	3519	36.7	-71.4	-25.1	1% Occipital Fusiform Gyrus
11	2675	1.13	19.4	58.2	51% Superior Frontal Gyrus
10	990	-45.2	20.9	-0.147	45% Frontal Operculum Cortex
9	531	44.6	21.1	-0.798	56% Frontal Operculum Cortex
8	495	-55.7	-49.1	36.4	44% Supramarginal Gyrus, posterior division
7	469	54.4	-47.6	42.8	51% Angular Gyrus
6	465	-24.6	52	27.3	47% Area 9/46D
5	308	-38.6	-63.9	-28.4	100% Left Crus I
4	265	-29.3	57.9	-11.1	92% FP1 (Lateral Frontal Pole)
3	28	-47.4	8.64	48.4	57% Area 8A
2	26	35.2	-95.1	9.08	23% Occipital Pole
1	20	-9	-87.3	-23.9	7% Occipital Fusiform Gyrus

Structures to which each cluster belongs to:

Cluster #12	Average Atlas Probability Within Cluster
Lateral Occipital Cortex, inferior division	9.1
Occipital Fusiform Gyrus	4.1
Occipital Pole	2.3

Cluster #11	Average Atlas Probability Within Cluster
Superior Frontal Gyrus	32.0
Paracingulate Gyrus	11.6

Cluster #10	Average Atlas Probability Within Cluster
Insular Cortex	7.4
Inferior Frontal Gyrus, pars triangularis	11.4
Inferior Frontal Gyrus, pars opercularis	14.0
Frontal Orbital Cortex	17.2
Frontal Operculum Cortex	9.9

Cluster #9	Average Atlas Probability Within Cluster
Area 44d	8.5
Area 44v	15.2
Area 45A	5.5
Area Fop (Frontal Operculum)	7.5

Cluster #8	Average Atlas Probability Within Cluster
Supramarginal Gyrus, posterior division	35.3
Angular Gyrus	20.5

Cluster #7	Average Atlas Probability Within Cluster
Supramarginal Gyrus, posterior division	23.2
Angular Gyrus	36.2

Cluster #6	Average Atlas Probability Within Cluster
Area 9/46D	32.4
Area 46	24.6
Area 8B	7.4

Cluster #5	Average Atlas Probability Within Cluster
Left VI	20.7
Left Crus I	68.9

Table 3. Atlas query of conjunction of Left Crus II connectivity results. For large clusters, sub-region labels are listed below. COG: Center of Gravity.

ClusterIndex	Voxels	COG X (mm)	COG Y (mm)	COG Z (mm)	COG Label
15	4622	-10.1	-40	51	35% Postcentral Gyrus
14	2876	60	-15.7	-16.1	45% Middle Temporal Gyrus, posterior division
13	2781	-25.8	-76.8	-38.4	88% Left Crus II
12	2397	15.9	41	40.8	55% Area 8B
11	1591	49.4	-58.4	35.7	36% Angular Gyrus
10	1349	28.7	-79	-33.8	91% Right Crus I
9	1211	-23.6	55.1	-7.96	96% FPl (Lateral Frontal Pole)
8	720	45.1	46	-8.95	55% Area 47
7	612	-63.3	-33.8	-7.68	76% Middle Temporal Gyrus, posterior division
6	563	-43.1	-64.6	44.7	54% Lateral Occipital Cortex, superior division
5	313	-43.1	16.7	42.1	39% Area 9/46V
4	281	-3.38	-56.4	-47.1	99% Left IX
3	174	-37.5	-22.8	14.9	25% Central Opercular Cortex
2	45	-63.6	-5.64	-27.1	17% Middle Temporal Gyrus, anterior division
1	39	33.7	21.6	-20.8	99% Fop (Frontal Operculum)

Structures to which each cluster belongs to:

Cluster #15	Average Atlas Probability Within Cluster
Precentral Gyrus	11.6
Postcentral Gyrus	16.5
Cingulate Gyrus, posterior division	13.3
Precuneous Cortex	18.3

Cluster #14	Average Atlas Probability Within Cluster
Temporal Pole	7.0
Superior Temporal Gyrus, posterior division	8.2
Middle Temporal Gyrus, anterior division	7.2
Middle Temporal Gyrus, posterior division	23.9
Middle Temporal Gyrus, temporooccipital part	4.7

Cluster #13	Average Atlas Probability Within Cluster
Left Crus I	25.6
Left Crus II	46.9

Cluster #12	Average Atlas Probability Within Cluster
Pre-Supplementary Motor Area	6.6
Area 9	7.9
Area 8B	10.0

Cluster #11	Average Atlas Probability Within Cluster
Angular Gyrus	28.5
Lateral Occipital Cortex, superior division	29.1

Cluster #10	Average Atlas Probability Within Cluster
Right Crus I	48.9
Right Crus II	33.4

Cluster #9	Average Atlas Probability Within Cluster
IFS (Inferior Frontal Sulcus)	7.6
FPl (Lateral Frontal Pole)	11.1
FPm (Medial Frontal Pole)	6.1

Cluster #8	Average Atlas Probability Within Cluster
Area 47	16.9
FPl (Lateral Frontal Pole)	6.7

Cluster #7	Average Atlas Probability Within Cluster
Superior Temporal Gyrus, posterior division	10.1
Middle Temporal Gyrus, posterior division	47.5
Middle Temporal Gyrus, temporooccipital part	5.3

Table 4. Atlas query of conjunction of Right Crus II connectivity results. For large clusters, sub-region labels are listed below. COG: Center of Gravity.

ClusterIndex	Voxels	COG X (mm)	COG Y (mm)	COG Z (mm)	COG Label
16	2775	28.1	-73.8	-40.5	96% Right Crus II
15	2573	-3.58	-49.1	31.6	76% Cingulate Gyrus
14	1901	-40.5	-69.7	36.9	51% Lateral Occipital Cortex, superior division
13	1873	-2.94	59.3	-0.838	41% Area 10
12	1183	-60.2	-48.6	-10.1	50% Middle Temporal Gyrus, temporooccipital part
11	982	-22.8	27.7	48.3	58% Area 8B
10	777	-59.3	-12	-15.4	33% Middle Temporal Gyrus, posterior division
9	484	3.45	-53.6	-48.1	95% Right IX
8	209	-37.7	35.1	-12.6	34% Frontal Orbital Cortex
7	163	-13.1	-87.5	-38.7	99% Left Crus II
6	44	-26.7	-17.1	-14.5	78% Left Hippocampus
5	27	-45.2	50.1	0.148	100% Area 46

Structures to which each cluster belongs to:

Cluster #16	Average Atlas Probability Within Cluster		
Right Crus I	18.4		
Right Crus II	50.4		
Cluster #15	Average Atlas Probability Within Cluster		
Cingulate Gyrus, posterior division	31.6		
Precuneous Cortex	33.5		
Cluster #13	Average Atlas Probability Within Cluster		
Area 10	23.5		
Frontal Medial Cortex	14.7		
Paracingulate Gyrus	7.0		
Cluster #12	Average Atlas Probability Within Cluster		
Middle Temporal Gyrus, posterior division	12.3		
Middle Temporal Gyrus, temporooccipital part	22.9		
Inferior Temporal Gyrus, temporooccipital part	14.4		
Cluster #11	Average Atlas Probability Within Cluster		
Cluster2 (PreSMA)	12.4		
Cluster10 (area 8B)	31.9		
Cluster #10	Average Atlas Probability Within Cluster		
Superior Temporal Gyrus, posterior division	9.4		
Middle Temporal Gyrus, anterior division	19.2		
Middle Temporal Gyrus, posterior division	25.4		
Cluster #8	Average Atlas Probability Within Cluster		
Frontal Pole	27.0		
Frontal Orbital Cortex	33.3		

Table 5. Atlas query of conjunction of Left Lobule VI connectivity results. For large clusters, sub-region labels are listed below. COG: Center of Gravity.

ClusterIndex	Voxels	COG X (mm)	COG Y (mm)	COG Z (mm)	COG Label
7	11282	38.5	-11.5	36.5	21% Precentral Gyrus
6	7523	-9.34	-59.6	-19.2	52% Left VI, 45% Left V
5	1709	-49.8	-1.52	18.6	18% Precentral Gyrus
4	190	16.4	-82.5	33.3	23% Cuneal Cortex
3	89	7.3	-37.2	-45.8	94% Brain-Stem
2	37	-7.46	-37.7	-43.7	82% Brain-Stem
1	23	-62.5	-19.7	35.5	56% Postcentral Gyrus

Structures to which each cluster belongs to:					
Cluster #17	Average Atlas Probability Within Cluster				
Precentral Gyrus	11.8				
Postcentral Gyrus	11.3				
Cluster #16	Average Atlas Probability Within Cluster				
Left V	8.0				
Left VI	13.9				
Left VIIIa	5.7				
Lingual Gyrus	12.1				
Cluster #15	Average Atlas Probability Within Cluster				
Insular Cortex	7.7				
Precentral Gyrus	26.2				
Central Opercular Cortex	13.2				
Cluster #14	Average Atlas Probability Within Cluster				
Lateral Occipital Cortex, superior division	24.1				
Cuneal Cortex	17.7				
Occipital Pole	5.9				

46

Table 6. Atlas query of conjunction of Right Crus II connectivity results. For large clusters, sub-region labels are listed below. COG: Center of Gravity.

ClusterIndex	Voxels	COG X (mm)	COG Y (mm)	COG Z (mm)	COG Label
5	12452	-39.1	-18.6	39.5	46% Postcentral Gyrus
4	6973	12.1	-57.7	-27.6	27% Lobule VI
3	618	56.1	-2.44	30.8	39% Precentral Gyrus
2	84	-40.9	37.3	21.4	50% Area 9/46V
1	72	0.556	-84.7	21.1	72% Cuneal Cortex

Structures to which each cluster belongs to:					
Cluster #5		Average Atlas Probability Within Cluster			
Precentral Gyrus		12.8616			
Postcentral Gyrus		13.9606			
Cluster #4		Average Atlas Probability Within Cluster			
Right V		8.8324			
Right VI		15.3594			
Right VIIIa		6.8124			
Lingual Gyrus		6.2613			
Cluster #3		Average Atlas Probability Within Cluster			
Precentral Gyrus		40.1392			
Postcentral Gyrus		14.2233			

Table 7. Areas of cortical surface activation during the relational processing task.

X	Y	Z	Glasser Region	X	Y	Z	Glasser Region
-43.16	51.75	-10.99	Left Area anterior 47r	46.72	44.85	20.86	Right Area posterior 9/46v
-45.71	51.13	-2.86	Left Area posterior 47r	38.97	30.76	-8.41	Right Anterior Ventral Insular Area
-51.39	26.05	5.63	Left Area 44	43.24	51.89	-12.2	Right anterior Area 47r
-42.94	34.55	39.16	Left Area 8C	45.57	52.54	-6.7	Right posterior Area 47r
-44.74	18.57	45.49	Left Area 8C	56.65	14.82	21.17	Right Rostral Area 6
-44.52	11.15	52.84	Left Area 55b	44.02	35.68	39.17	Right Area 8C
-36.33	24.07	55.72	Left Ventral Area 8A	46.16	18.2	42.59	Right Area 8C
-11.94	16.88	66.78	Left Superior Frontal Language Area	38.57	24.27	55.31	Right Area 8Av
-5.96	28.69	48.5	Left Area 8B medial	36.42	16.7	59.66	Right Inferior 6-9 Transitional Area
-51.51	-52.34	49.8	Left Area PFm Complex	6.6	29.18	48.98	Right Area 8B medial
-42.38	-68.67	49.15	Left Area PFm Complex	59.89	-33.48	46.96	Right Area PF Complex
-7.77	-72.25	41.87	Left Parieto-Occipital Sulcus Area 2	52.36	-39.92	50.31	Right Area IntraParietal 2
-15.61	-90.05	-13.56	Left Second Visual Area	55.99	-41.9	48.7	Right Area PFm Complex
-28.53	-83.15	-17.26	Left Fourth Visual Area	45.79	-52.63	50.2	Right Area IntraParietal 2
-10.04	-95.63	0	Left Primary Visual Cortex	46.83	-63.46	48.24	Right Area PFm Complex
-10.63	-97.52	13.78	Left Second Visual Area	40.08	-68.04	48.98	Right Area IntraParietal 1
-19.14	-100.1	14.97	Left Third Visual Area	29.31	-72.5	49.12	Right Medial IntraParietal Area
-	-	-	-	32	-78.71	-17.04	Right Eighth Visual Area
-	-	-	-	24.99	-82.21	-12.27	Right Fourth Visual Area
-	-	-	-	19.1	-88.21	-12.27	Right Second Visual Area
-	-	-	-	21.72	-86.92	-13.33	Right Third Visual Area
-	-	-	-	13.74	-94.47	-0.07	Right Primary Visual Cortex
-	-	-	-	14.69	-96.49	15.02	Right Second Visual Area
-	-	-	-	20.43	-97.23	18.69	Right Third Visual Area

Note: XYZ Coordinates are reported in inflated cortical surface space. More information about Glasser Parcellation areas can be found in the supplementary neuroanatomical results of Glasser et al. (2016).

Table 8. Areas of cortical surface activation during the working memory task.

X	Y	Z	Glasser Region	X	Y	Z	Glasser Region
-34.85	58.97	16.09	Left Area 9-46d	28.27	64.59	5.47	Right Area posterior 10p
-44.03	38.96	31.78	Left Area posterior 9-46v	34.62	59.54	16.39	Right Area 9/46d
-37.12	30.49	-6.76	Left Anterior Ventral Insular Area	39.61	58.47	9.99	Right Area anterior 9/46v
-5.95	26.92	49.36	Left Area 8B medial	30.19	45.97	40.11	Right Area 46
-6.06	16.42	54.42	Left Supplementary and Cingulate Eye Field	44.53	42.52	30.86	Right Area posterior 9/46v
-17.12	13.72	68.38	Left Area 6m anterior	39.06	30.76	-7.3	Right Anterior Ventral Insular Area
-46.58	13.31	44.17	Left Area 8C	39.42	27.32	1.93	Right Frontal Opercular Area 4
-29.22	9.24	61.81	Left Area 6 anterior	6.58	26.37	49.36	Area 8B medial
-42.29	-54.92	50.43	Left Anterior IntraParietal Area	52.25	25.09	4.8	Right Area 44
-49.97	-55.28	49.82	Left Area PFcm	6.72	18.26	52.45	Right Supplementary and Cingulate Eye field
-7.72	-67.22	53.36	Left Medial Area 7P	26.82	17.38	60.21	Right Area 6 anterior
-	-	-	-	36.48	15.05	60.09	Right Inferior 6-8 Transitional Area
-	-	-	-	57.61	14.56	18.37	Right Rostral Area 6
-	-	-	-	20.77	11.98	68.41	Right Area 6m anterior
-	-	-	-	31.75	6.44	61.87	Right Area 6 anterior
-	-	-	-	59.83	-34.61	46.89	Right Area PF Complex
-	-	-	-	56.03	-42.85	48.38	Right Area PFm Complex
-	-	-	-	42.21	-46.17	51.76	Right Anterior IntraParietal Area
-	-	-	-	49	-46.74	50.09	Right Area IntraParietal 2
-	-	-	-	8.72	-66.97	53.48	Right Medial Area 7P
-	-	-	-	41.45	-67.28	48.92	Right Area IntraParietal 1
-	-	-	-	45.3	-78.8	36.49	Right Area PGs

Note: XYZ Coordinates are reported in inflated cortical surface space. More information about Glasser Parcellation areas can be found in the supplementary neuroanatomical results of Glasser et al. (2016).

Table 9. Areas of cortical surface activation during the language task.

X	Y	Z	Glasser Region	X	Y	Z	Glasser Region
-9.72	54.44	35.73	Left Area 9 middle	8.91	47.73	-11.29	Right Area 10r
-8.15	46.52	-18.05	Left Area 10v	9.39	46.47	-14.32	Right Area 10v
-9.82	41.41	50.38	Left Area 8B lateral	37.38	42.16	-17.64	Right Area 47m
-48.98	40.76	-3.85	Left Area 45	44.73	40.9	-13.42	Right Area 47 lateral
-42.26	39.44	-14.3	Left Area 47 lateral	54.04	35.74	7.74	Right Area 45
-6.25	36.95	-11.92	Left Area s32	49.56	12.08	-35.26	Right Area TG dorsal
-41.22	20.77	53.34	Left Area 8Av	60.83	-5.04	-18.32	Right Area STSd anterior
-8.73	19.1	63.65	Left Superior Frontal Language Area	61.21	-7.92	-7.81	Right Area A4
-47.84	13	-33.7	Left Area TG dorsal	4.27	-52.66	25.2	Right Area ventral 23 a+b
-48.07	6.49	-37.9	Left Area TG dorsal	6.72	-61.61	37.88	Right Area 7m
-44.82	0.39	-42.08	Left Area TG ventral	55.28	-69.93	27.47	Right Area PGi
-57.7	-4.17	-19.03	Left Area STSv anterior	-	-	-	-
-59.11	-7.74	-24.05	Left Area TE1 anterior	-	-	-	-
-58.92	-8.52	-11.35	Left Area STSd anterior	-	-	-	-
-42.69	-14.08	-37.03	Left Area TF	-	-	-	-
-58.88	-38.28	-0.88	Left Area STSd posterior	-	-	-	-
-60.25	-41.97	-2.26	Left Area STSv posterior	-	-	-	-
-7.06	-53.16	41.15	Left Area 31pd	-	-	-	-
-50.7	-69.6	28.33	Left Area PGi	-	-	-	-

Note: XYZ Coordinates are reported in inflated cortical surface space. More information about Glasser Parcellation areas can be found in the supplementary neuroanatomical results of Glasser et al. (2016).

X	Y	Z	Glasser Region
Table 10. Areas of cortical surface activation during the motor task.			
-6.01	-7.31	55.95	Left Dorsal Area 24d
-35.6	-14.14	68.77	Left Dorsal Area 6
-37.86	-18.7	65.41	Left Area 4
-48.39	-19.02	54.7	Left Primary Sensory Cortex
-54.06	-19.48	52.11	Left Area 1
-37.86	-24.06	62.07	Left Area 3a
-40.81	-33.98	66.9	Left Area 1

Note: XYZ Coordinates are reported in inflated cortical surface space. More information about Glasser Parcellation areas can be found in the supplementary neuroanatomical results of Glasser et al. (2016).

Figure Legends

Figure 1. Peak activations from the four functional tasks: working memory (red), relational processing (blue), language (green), and motor (yellow) overlaid on the inflated cortical surface (top row in each section) and the cerebellum (bottom row in each section). Cluster-corrected activation maps were further thresholded at the 95 percentile to isolate peaks of activation, and were binarized for display. The working memory activation was thresholded at T>10.98, relational processing was thresholded at T>9.34, language was thresholded at T>15.5, and motor was thresholded at T>13.45.

Figure 2. Comparison of resting-state connectivity for left cerebellar seeds. Seeds were derived from the SUIT Probabilistic Cerebellar Atlas and included Crus I, Crus II, and Lobule VI. Pairwise comparisons for seed-to-voxel connectivity were created with linear contrasts in CONN that included all three seeds and setting the weight for the third seed that was not of interest to 0, e.g., for the contrast of Left Crus I > Left Crus II, the weight for Left Lobule VI was set to 0, i.e., [1 -1 0].

Figure 3. Comparison of resting-state connectivity for right cerebellar seeds. Seeds were derived from the SUIT Probabilistic Cerebellar Atlas and included Crus I, Crus II, and Lobule VI. Pairwise comparisons for seed-to-voxel connectivity were created with linear contrasts in CONN that included all three seeds and setting the weight for the third seed that was not of interest to 0, e.g., for the contrast of Right Crus I > Right Crus II, the weight for Right Lobule VI was set to 0, i.e., [1 -1 0].

Figure 4. Relational processing related cortical surface activation (left) and cerebellar volumetric activation (right). Results come from a group-level analysis of the contrast of relational vs. match for the Relational Processing Task.

Figure 5. Working memory related cortical surface activation (left) and cerebellar volumetric activation (right). Results come from a group-level analysis of the contrast of 2-back vs. 0-back trials for the N-Back Task.

Figure 6. Language related cortical surface activation (left) and cerebellar volumetric activation (right). Results come from a group-level analysis of the contrast of story vs. math trials in the Story Task.

Figure 7. Motor related cortical surface activation (left) and cerebellar volumetric activation (right). Results come from a group-level analysis of the contrast of right hand vs. baseline trials in the Motor Tapping Task.

Figure 8. Peak activations from the four functional tasks: working memory (red), relational processing (blue), language (green), and motor (yellow) overlaid on the inflated cortical surface (top row in each section) and the cerebellum (bottom row in each section). Cluster-corrected activation maps were further thresholded at the 95 percentile to isolate peaks of activation, and were binarized for display. The working memory activation was thresholded at T>10.98, relational processing was thresholded at T>9.34, language was thresholded at T>15.5, and motor was thresholded at T>13.45.